Journal of Alloys and Compounds 668 (2016) 187–193

Contents lists available at ScienceDirect

Journal of Alloys and Compounds

journal homepage: http://www.elsevier.com/locate/jalcom

Structural characterization of epitaxial $LiFe_5O_8$ thin films grown by chemical vapor deposition

B. Loukya [a, b], D.S. Negi [a, b], R. Sahu [a, b], N. Pachauri [c], A. Gupta [c], R. Datta [a, b, *]

[a] International Centre for Materials Science, Jawaharlal Nehru Centre for Advanced Scientific Research, Bangalore, 560064, India
[b] Chemistry and Physics of Materials Unit, Jawaharlal Nehru Centre for Advanced Scientific Research, Bangalore, 560064, India
[c] Center for Materials for Information Technology, University of Alabama, Tuscaloosa, Alabama, 35487, USA

ARTICLE INFO

Article history:
Received 20 November 2015
Received in revised form
23 January 2016
Accepted 27 January 2016
Available online 29 January 2016

Keywords:
Chemical vapor deposition
Epitaxial $LiFe_5O_8$ thin films
Structural ordering
Transmission electron microscopy

ABSTRACT

We report on detailed microstructural and atomic ordering characterization by transmission electron microscopy in epitaxial $LiFe_5O_8$ (LFO) thin films grown by chemical vapor deposition (CVD) on MgO (001) substrates. The experimental results of LFO thin films are compared with those for bulk LFO single crystal. Electron diffraction studies indicate weak long-range ordering in LFO (α-phase) thin films in comparison to bulk crystal where strong ordering is observed in optimally annealed samples. The degree of long-range ordering depends on the growth conditions and the thickness of the film. Annealing experiment along with diffraction study confirms the formation of α-Fe_2O_3 phase in some regions of the films. This suggests that under certain growth conditions γ-Fe_2O_3-like phase forms in some pockets in the as-grown LFO thin films that then convert to α-Fe_2O_3 on annealing.

1. Introduction

Lithium ferrite, $Li^{1+}_{0.5}Fe^{3+}_{2.5}O^{2-}_4$ or $LiFe_5O_8$ (LFO), is a ferrimagnetic spinel oxide with large saturation magnetic moment (2.5 μ_B/unit cell) and Curie temperature (950 K) [1]. LFO offers several important technological applications, e.g., electrode for rechargeable lithium ion batteries, magnetic insulators for spin filtering in spintronics, various components in microwave devices, etc. [2–8]. LFO is reported to occur in two crystallographic forms, ordered α-LFO (space group $P4_132/P4_332$) and disordered β-LFO (space group $Fd\bar{3}m$) [1]. Further, the α-LFO phase can exist in two enantiomorphic forms, where each form was reported to split into four domains related to each other by ½ <110> translation of the f.c.c cell [9]. The ordered LFO has lattice parameters $a = c = 8.33$ Å, in which the Li and Fe cations are ordered in a 1:3 periodic chains along the [110] quasi-cubic directions. In this ordered structure, Fe^{3+} occupies octahedral 12d and tetrahedral 8c Wyckoff position and Li^+ ions occupy only the octahedral 4b position. The disordered LFO phase also has an inverse spinel structure but with Fe^{3+} cations at the tetrahedral 8a positions and a mixture of Li^+ and Fe^{3+} in 1:3 ratio at the octahedral 16d positions [10,11]. The order-disorder transformation occurs at ~750 °C and the disordered phase can be kinetically stabilized by rapid quenching [1]. Only few reports exist in the literature on the characterization of the two forms of this material, mostly carried out by X-ray, Raman, Mössbauer, and IR spectroscopic methods [12]. In comparison to these techniques, electron diffraction carried out in a transmission electron microscope is more effective and extremely sensitive in providing direct information on the ordering state due to strong Coulomb interaction between the probe electrons and atoms. Additionally, imaging in TEM provides detailed information on the defect structures in the films.

LFO epitaxial thin films grown on different substrates such as MgO, $MgAl_2O_4$ (MAO) and $SrTiO_3$ (STO) were characterized in terms of epitaxial quality, strain and magnetic properties [13]. LFO on MgO grows under compressive stress and under tensile stress on MAO and STO substrates. The surface quality is found to be superior on MgO substrates. On the other hand, magnetic properties were found to be better for films grown on MAO substrates. Raman spectroscopy interpreted the comparatively poor magnetic properties resulting from disordered β-LFO phase for films grown on MgO. However, in the present report, electron diffraction studies shows clear evidence of ordering in epitaxial LFO films grown on (100)-oriented MgO substrates and the ordering is found to be of weak long-range or intermediate-range as compared to short or long-range ordering found in bulk single crystals depending on the

* Corresponding author. International Centre for Materials Science, Jawaharlal Nehru Centre for Advanced Scientific Research, Bangalore, 560064, India.
E-mail address: ranjan@jncasr.ac.in (R. Datta).

http://dx.doi.org/10.1016/j.jallcom.2016.01.217
0925-8388/

thermal treatment [14]. Interestingly, the ordering is observed to disappear (disappearance of superlattice spots) within couple of minutes under electron beam irradiation (supporting videos showing the time series of HRTEM and the corresponding FFT). Annealing the films and crystals above 750 °C followed by air cooling confirm the formation of completely disordered β-LFO phase. Under certain growth conditions some regions of the LFO film are found to show symmetry close to γ-Fe_2O_3 -like phase and this transforms to α-Fe_2O_3 -like phase upon annealing. Besides electron diffraction, electron energy loss spectroscopy (EELS) has also been utilized to distinguish the α-Fe_2O_3 phase from the surrounding β-LFO phase after annealing. The results reported in this manuscript add to the present understanding of lithium ferrite, particularly in the form of epitaxial thin films.

Supplementary data related to this article can be found online at http://dx.doi.org/10.1016/j.jallcom.2016.01.217.

2. Experimental techniques

The different LFO thin film samples investigated by transmission electron microscopy (TEM) are summarized in Table 1. Films for the present study were grown on (100) MgO substrate using direct liquid injection chemical vapor deposition (DLI-CVD) technique. The DLI-CVD reactions were performed in a horizontal quartz-tube, reactor furnace. The tube reactor was pumped down to the reaction pressure of 3.5 Torr by a rotary vane vacuum pump. For film growth anhydrous Li(acac) and $Fe(acac)_3$ (acac: acetylacetonate) in a molar ratio of 1:5 were dissolved in N,N-dimethylformamide (DMF) to form a clear homogeneous precursor solution without any further purification. DMF serves as a solvent and can simultaneously minimize intermolecular association by coordinating with the metal ions. Ultrahigh-purity He (20 psi) was used to pressurize the liquid flow from the solution container to a Brooks Instrument DLI 200 vaporizer system. The flow rate of the liquid solution was controlled by liquid massflow controller and was set to 8 g/h during the reaction. An ultrahigh-purity argon gas with a flowrate of 300 sccm was used as the carrier gas, which served both as the vaporization medium and the delivery gas. At the vaporizer inlet, where the liquid and carrier gas flow intersect, was an atomizer, which breaks up the entering fluid into fine droplets (2~5 μm) because of a large pressure drop. Because of efficient heat and mass transport between the fine droplets and the pre-heated (175 °C) carrier gas (Ar), the metal-organic precursors becomes homogenously entrained in the solvent vapor and carried into the reactor without premature decomposition. Ultrahigh-purity oxygen with a flow rate of 150 sccm was used as the oxidant. Prior to the reaction, the MgO substrates were ultrasonically cleaned sequentially in acetone and isopropanol, and then blow dried with N_2. After deposition, the films were slowly cooled to room temperature at the rate of 1.5 °C per minute in the reactor under flowing O_2. Thin film LFO samples were deposited at an optimized substrate position in the furnace for temperatures ranging from 400 °C to 650 °C with varying thicknesses to study the effect of these two parameters on the ordering state of LFO. All the other optimized growth parameters, such as flow rate and vaporization temperature of precursor solutions, flow rate of O_2, and the total pressure in the reactor, were kept constant for all films. The details regarding the bulk crystal growth can be found in Ref.14.

Table 1
Details on the growth temperature and thickness of various LFO samples from TEM studies.

Sample	Growth temperature (°C)	Thickness (nm)
LFO_1/MgO	450	230
LFO_2/MgO	500	130
LFO_3/MgO	500	140
LFO_4/MgO	550	130
LFO_5/MgO	600	350
LFO_6/MgO	600	1000
LFO_6 (Annealed)	600	1000
LFO_single crystal	980	NA

The samples were characterized by X-ray diffraction in Philips X'pert Pro, Cu Kα source to determine the epitaxial quality, lattice parameter and strain in the thin films. TEM samples were prepared by mechanical polishing followed by Ar ion milling to prepare large electron transparent thin area. Diffraction contrast imaging, high resolution imaging and recording of electron diffraction patterns were performed in an aberration corrected FEI TITAN^{3TM} 80–300 kV TEM. Sample thickness was determined from cross-sectional TEM images. High resolution electron energy loss spectroscopy of O *K* edge and Fe $L_{3,2}$ edge were acquired using a gun monochromator. The best energy resolution obtainable using gun monochromator was better than 0.18 eV at relatively higher magnification and smallest GIF entrance aperture. However, for recording the absorption edges the resolution was compromised to ~0.25 eV by reducing the magnification in order to ensure good signal [15]. Density functional theory based calculations were performed using WIEN2k [16], a full potential linear augmented plane wave method to calculate the crystal properties. In order to calculate the cohesive energy of the LFO and γ-Fe_2O_3 (maghemite structure), unit cells with space group $P4_332$ with respective lattice parameter of a = 8.42 Å and 8.405 Å were considered [13]. The structure was fully relaxed using PBE exchange correlation functional with the convergence criteria of energy ~0.0001Ry, force ~1 mRh/au and charge ~0.001 or below. Core and the valance states were separated by the energy gap of −6 Ry. $R_{mt}K_{max}$ parameter was set to 7. A dense mesh of 10 × 10 × 10 k-point was considered in the first Brillouin zone for energy convergence in the self-consistent field cycle calculation. The GGA exchange correlation underestimates the band gap for transition metal oxides, therefore to improve the estimation of the band gap, we employed the recently developed modified Becke-Johnson (mBJLDA) potential as implemented in WIEN2K package [17].

3. Results and discussion

Table 1 summarizes the growth temperature and thickness of the thin films and bulk crystal investigated for cation ordering through electron diffraction patterns and defects by strain contrast imaging in TEM. X-ray diffraction data for LFO films grown at temperatures between 450 °C and 600 °C exhibit pure spinel phase structure without any additional peaks, as only (400) and (800) peaks from the lithium ferrite film are observed in the normal θ- 2θ scans. The room temperature crystallographic data provide clear evidence of good epitaxial quality and the presence of significant strain in all the LFO films of varying thicknesses grown on MgO substrates. This is shown in Fig. 1 for films grown at different temperatures, where the dotted line indicates the bulk 2θ peak position of LFO (400) reflection. There is stress induced by the substrate, which is not completely relaxed by misfit dislocations at the interface between film and substrate. A systematic shift of the film peak to lower angles, towards the bulk value, is observed with increasing deposition temperature. In order to determine the in-plane lattice parameters, diffraction scans were also performed on the (110) planes with appropriate tilting of the substrates. Example lattice parameters for 500 °C (LFO_2) and 600 °C (LFO_5) films are c = 8.281, a = 8.424 Å and c = 8.316, a = 8.395 Å, respectively.

Fig. 2 shows example TEM bright field images for LFO_2 and

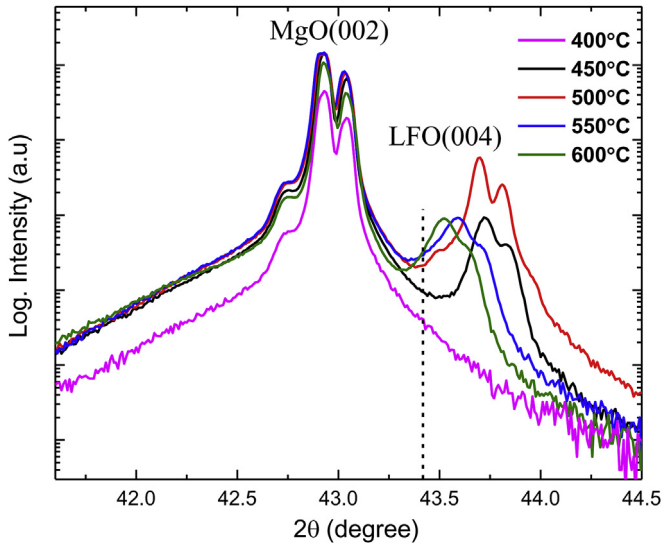

Fig. 1. 2θ–θ plot around the (004) peak for LFO films grown at different temperatures exhibiting a pure spinel phase with the (h00) planes parallel to the film surface. The bulk value for LFO is marked as dashed line.

the appearance of the spots and their numbers in some of the diffraction patterns. Fig. 3(c) is the diffraction pattern from LFO thin film (LFO_2) showing superlattice spots at ¼ g_{400} periodicity. This is the usual Li/Fe ordering with $P4_332$ space group symmetry already described. However, for the as-grown single crystal and some of the films, particularly close to the surface regions, the ½ g_{400} superlattice spots are missing. This is due to the short-range nature of the ordering. For the single crystal, strong ordering is observed only after annealing the crystal [13]. Similar feature associated with the short range ordering has been observed previously in other material systems, e.g., $RE_{0.5}(Ca_{1-y}Sr_y)_{1.5}MnO_4$ (RE = Pr, Eu) where superlattice spots associated with the charge order/orbital order changes from the long-range commensurate structure to short-range incommensurate structure with increase in Sr incorporation [20]. The difference in diffraction pattern associated with short-range ordering between the films and single crystal is the sharpness of the spots. In the case of films, weak long-range ordering exist as the ½ g_{400} superlattice spots are weak but are still visible and these spots are completely missing in the as-grown bulk crystal. Raman spectroscopy of LFO films grown on MgO by pulsed laser deposition suggested the presence of disorder [19]. However, the present electron diffraction study of CVD-grown films

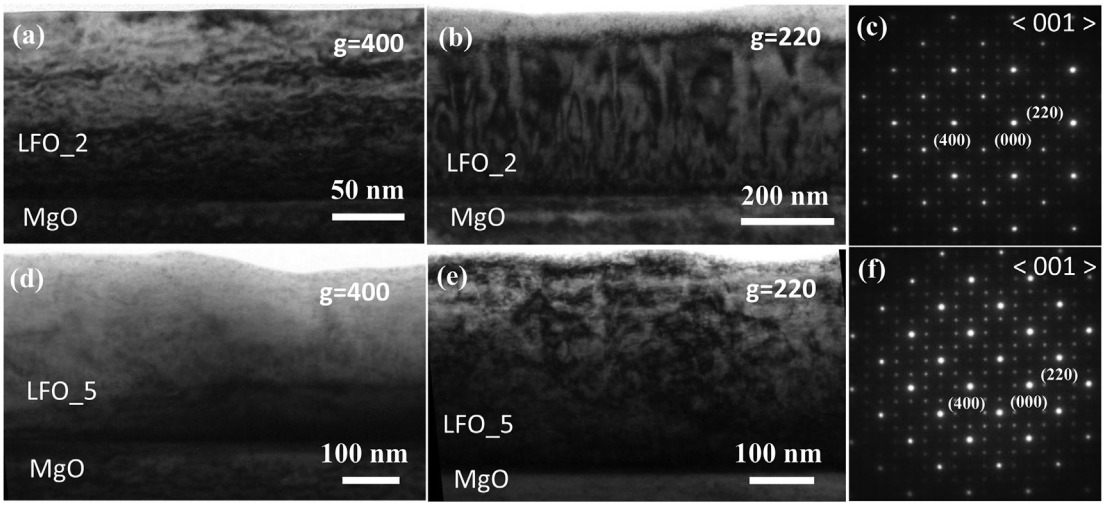

Fig. 2. (a) & (b) are the TEM bright field images for LFO_2 film with g = 400 and 220 reflections, respectively. (c) Electron diffraction pattern from LFO_2 along <001> zone axis. (d) & (e) Bright field images from LFO_5 with g = 400 and g = 220, respectively. (f) Corresponding electron diffraction pattern from LFO_5 along <001>. The electron diffraction patterns indicate that the films are epitaxial and strained to match with the substrate.

LFO_5 films with g = <400> and g = <220> diffracting vectors. The corresponding <100> zone axis electron diffraction patterns from the films are shown in Fig. 2 (c) & (f). Bright field images of the remaining samples can be found in the supporting information. From the electron diffraction patterns (from the film and substrate together) it is clear that the films are grown under strain. Films with thickness higher than 500 nm, i.e. LFO_2 and LFO_5, are partially relaxed as one can observe the presence of threading dislocations (Fig. 2). Other than threading dislocations, dark diffused contrast areas can also be observed and this may be related to either anti-phase domains or *A* site cation vacancies [18,19]. Fig. 3 shows the electron diffraction patterns taken from various thin films grown at different temperatures and from the bulk crystal. One can notice the presence of superlattice diffraction spots (weak intensity) present in between the primary diffraction spots (strong intensity). The appearance of superlattice spots is due to Li/Fe ordering at the octahedral sites of the structure. One can also notice differences in shows clear short-range ordering and weak long-range ordering. The electron diffraction study is consistent with a previous report where it was shown by Mössbauer studies that in weakly substituted LFO a partial order/short-range order always exists [12].

The observation of 1/12 g_{400} SL periodicity from some areas in the upper surface layer of LFO_1 film (Fig. 4) is surprising. This kind of periodicity has two possible origins. It is either due to the presence of vacancy-ordered maghemite structure (γ-Fe_2O_3 phase) or α-LFO having similar periodicity as γ-Fe_2O_3 phase. The possibility of the former can be expected based on energy considerations (cohesive energies: LFO = 6.625 eV/atom; maghemite = 6.848 eV/atom) [21]. The accumulation of vacancies in pockets of LFO might favor the formation of γ-Fe_2O_3 like phase in the LFO background. α-LFO has a space group $P4_332$, where there are two types of octahedral sites. One type of octahedral site has multiplicity of 4 and the other has multiplicity of 12 in the unit cell. For α-LFO it is the octahedral position with multiplicity 4 which is occupied by Li.

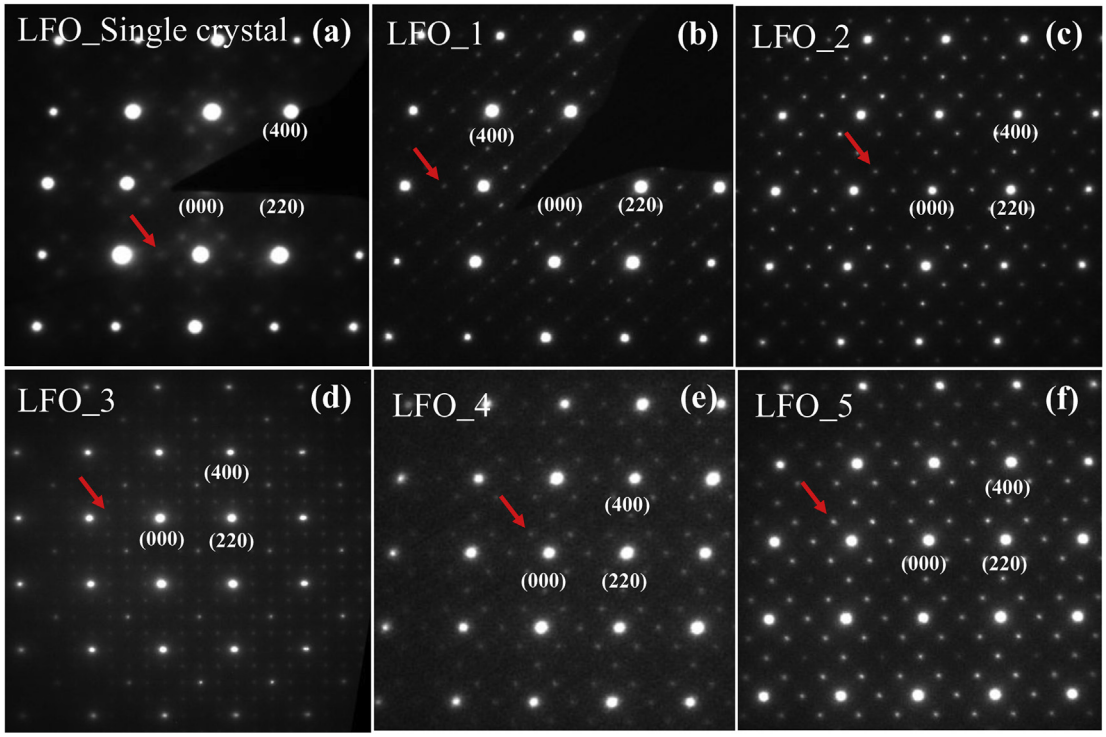

Fig. 3. Electron diffraction patterns along <001> zone axis from various LFO samples grown at different temperatures as listed in Table 1. The superlattice spots in each pattern are marked with red arrow. (For interpretation of the references to colour in this figure legend, the reader is referred to the web version of this article.)

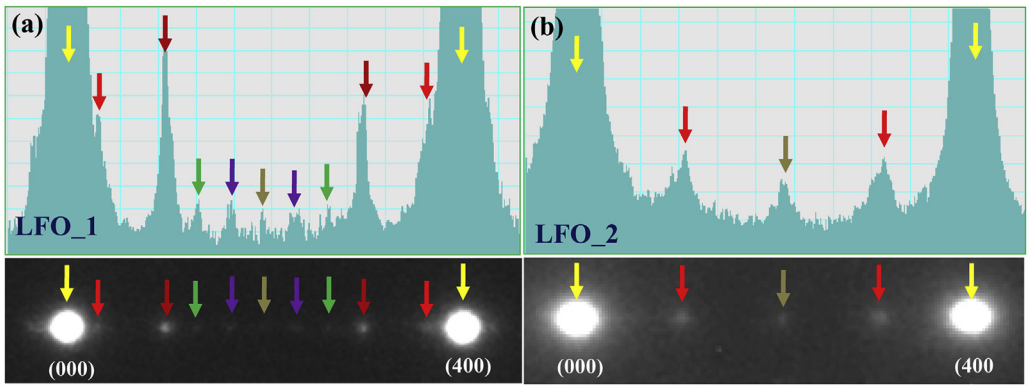

Fig. 4. Line profiles of the electron diffraction spots between g = (000) and g = (400) obtained from LFO_1 and LFO_2. (a) The appearance of higher order superlattice spots of (1/12) g_{400} from LFO_1 is clearly visible. (b) Superlattice spots of only (1/4)g_{400} is visible from LFO_2.

However, vacancy ordered γ-Fe_2O_3 phase has the tetragonal space group $P4_12_12$ with $a = 8.347$ Å and $c = 25.042$ Å. This spinel tetragonal superstructure with $c/a = 3$ (spinel cubic cell is tripled along the c-axis), where the Fe atoms are completely ordered (vacancy to Fe in 1:5 ratio at the octahedral interstices), has been confirmed both by neutron and synchrotron X-ray diffraction studies [22–24]. This latter possibility has already been described in Ref. 25. This $P4_12_12$ tetragonal space group is fully ordered compared to $P4_332$, where disorder exists to some extent as the 4b sites have fractional iron occupancy. Therefore the observed 1/12 g_{400} SL periodicity from some of the pockets in top layer of LFO_1 film might be due to the formation of γ-Fe_2O_3 phase, which is subsequently confirmed by annealing experiments described in the next paragraph. In the calculated diffraction pattern there are many spots missing systematically. However, we see these missing spots in the experimental electron diffraction pattern. This is due to the co-existence of the α-LFO and γ-Fe_2O_3 phases in the same pattern. These are marked in Fig. 5.

In order to conclusively determine the origin of 1/12 g_{400} SL periodicity, whether it is due to γ-Fe_2O_3 phase or α-LFO having similar periodicity as γ-Fe_2O_3, we have additionally carried out annealing experiment of the film at 750 °C for 1 h in normal atmosphere followed by air cooling along with similar annealing schedule of a bulk single crystal. The phase transition temperature for γ-Fe_2O_3 to α-Fe_2O_3 is around 400 °C and the annealing temperature used is much higher than the phase transition temperature, thus complete phase transformation can be expected. Formation of γ-Fe_2O_3 is a result of the loss of Li_2O from LFO. Such regions can precipitate out during the annealing process to result in the formation of γ-Fe_2O_3 which is a more stable phase [8,25]. We find that after annealing the structure transforms from ordered α-LFO to disordered β-LFO phase for both the film and bulk sample.

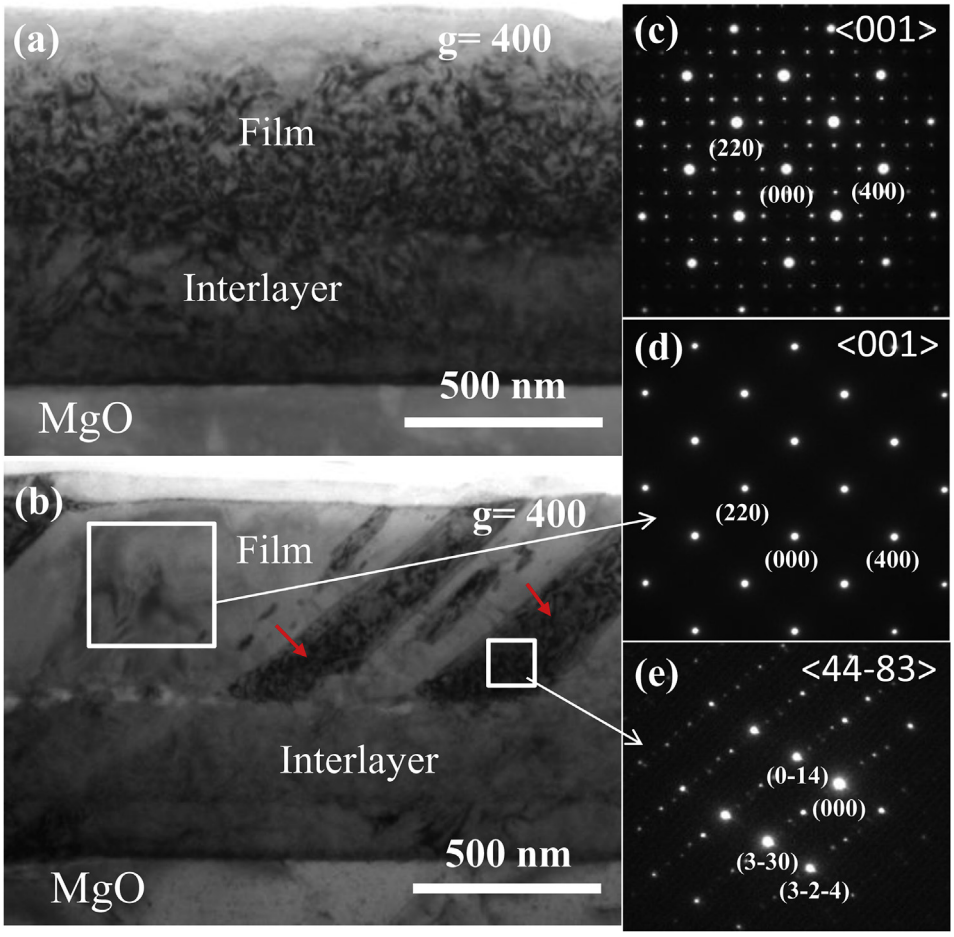

Fig. 5. Experimental bright field TEM images from LFO thin films (a) before and (b) after annealing. (c) Electron diffraction pattern from the film before annealing. (d) Diffraction pattern from the film region clearly show the disappearance of ordering on annealing. The arrows in red color indicate the regions of the film that has undergone re-crystallization to α-Fe_2O_3 like phase and the corresponding diffraction pattern from such regions is shown in (e). (For interpretation of the references to colour in this figure legend, the reader is referred to the web version of this article.)

This is evident from the disappearance of SL spots (Fig. 5). However, one can observe some areas of re-crystallization as marked with the arrows (red color) in Fig. 5(b). While performing selected area electron diffraction from such regions (shown in Fig. 5(b)), it is found that the structure transforms to some trigonal/hexagonal phase and the diffraction analysis corresponds to the α-Fe_2O_3 phase with $a = 5.19$ Å and $c = 13.75$ Å (Fig. 5), which matches well with the previously published reports [25,26]. Schematic of ordered γ-Fe_2O_3 or α-LFO and α-Fe_2O_3 are shown in Fig. 6. Vacancy sites in the tetragonal γ -Fe_2O_3 shown by green spheres are occupied by Li atoms in ordered LFO. We also have performed scanning transmission electron microscopy (STEM) and energy dispersive X-ray spectroscopy (EDX) line profiling to confirm that there is no inter diffusion of Mg into the film at such high annealing temperatures as shown in Fig. 7. The appearance of contrast in the top part of the annealed sample in Fig. 5 is due to the strain contrast and re-crystallization of the sample in those regions. The magnified bright field image is provided in the supplementary document. High resolution EELS spectra of Fe $L_{2,3}$ absorption edge have been acquired from thin films and bulk crystals before and after annealing and also from the possible α-Fe_2O_3 phase in the annealed sample. The spectra are compared in Fig. 8. There is no change in the spectral shape and fine features in films and bulk crystals before and after annealing as indicated with the arrow. But the film LFO_6 before and after annealing shows a clear difference in the pre-edge

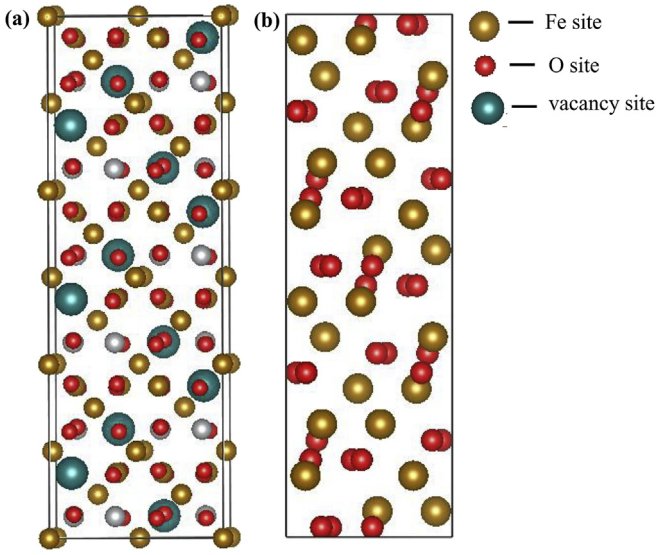

Fig. 6. Schematic structures of ordered (a) γ-Fe_2O_3 or α-LFO and (b) α-Fe_2O_3. Vacancy sites in the tetragonal γ -Fe_2O_3 are indicated by green spheres. These sites are occupied by Li atoms in ordered LFO. (For interpretation of the references to colour in this figure legend, the reader is referred to the web version of this article.)

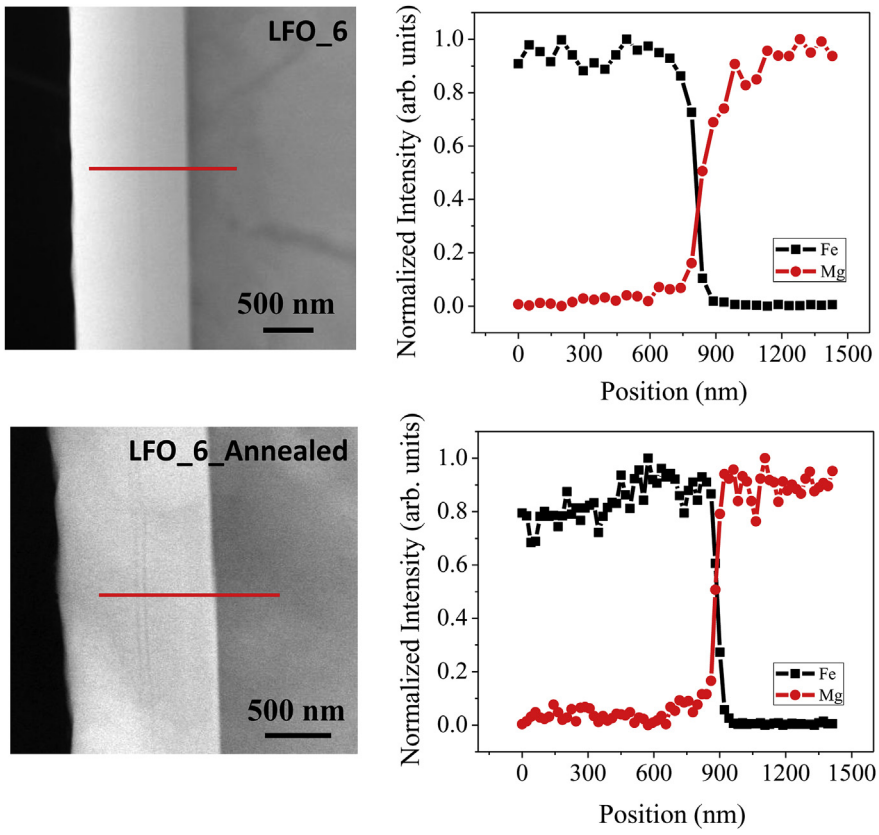

Fig. 7. STEM-EDX line profile from LFO_6 sample before and after annealing indicating no Mg diffusion across the film–substrate interface.

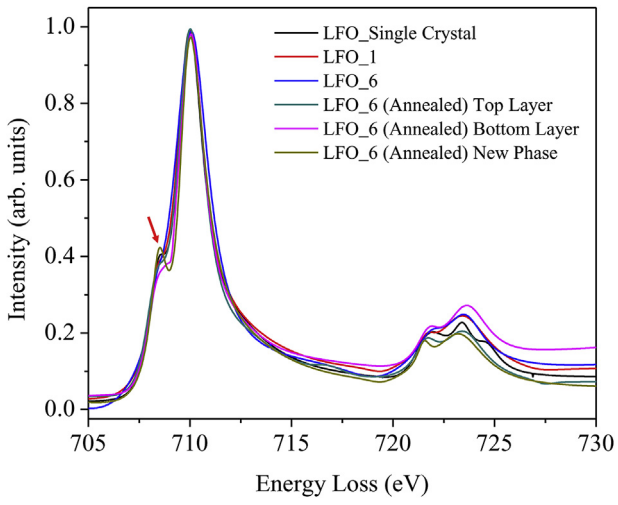

Fig. 8. Electron energy loss spectra of Fe $L_{2,3}$ from bulk single crystal, LFO_1, LFO_6 thin films, and also from various regions of the LFO_6 film after annealing. The spectra from the regions of α-Fe_2O_3 phase shows increase in peak intensity as marked with the arrow.

spectral feature. After annealing, the pre edge spectral feature is clearer, indicating an increase in the number of octahedral sites compared to the tetrahedral sites in the structure in some pockets [27]. This also supports the formation of α-Fe_2O_3 after annealing. The spectra resemble LFO structure and for Fe $L_{2,3}$ edge it is a mixture of tetrahedral and octahedral geometry. For α-Fe_2O_3 regions the spectral shape is distinct compared to LFO.

An important point of the electron diffraction study is that it reveals weak long range ordering in the strained LFO thin films grown on MgO substrate, while previous X-ray and Raman spectroscopy techniques could not yield such information and incorrectly assigned the structure to disordered β-LFO phase [13]. Innovations in growth strategy in terms of cooling rate might render films with strong ordering which are expected to exhibit magnetic properties close to bulk material. The ordering is observed to disappear after a few minutes of electron beam exposure due to highly mobile Li atoms in the structure and one can also use this method to stabilize disordered β-LFO phase at room temperature instead of rapid quenching from higher phase transition temperature [Supplementary Information].

4. Conclusions

$LiFe_5O_8$ thin films grown on MgO (001) substrates by CVD at different growth temperatures and different thicknesses are studied by transmission electron microscopy for epitaxial and atomic ordering characterization. The films are strained and show intermediate-range ordering as compared to long-range ordering obtained for optimally annealed bulk crystals. The electron diffraction results are in contrast to previously assigned disordered β-LFO phase by Raman spectroscopy and innovation in growth methods to enhance the ordering will lead to magnetic properties close to bulk counterpart. Electron diffraction and electron energy loss spectroscopy studies reveal the presence of α-Fe_2O_3 phases upon annealing, indicating possibility of formation of γ-Fe_2O_3 in certain regions of the as-grown films.

Acknowledgments

The authors at JNCASR sincerely acknowledge Prof. C. N. R. Rao for his constant support and for providing the advanced microscopy facility for this research. The work at the University of Alabama was supported by NSF Grant No.ECCS-1509875.

Appendix A. Supplementary data

Supplementary data related to this article can be found at http://dx.doi.org/10.1016/j.jallcom.2016.01.217.

References

[1] P.B. Braun, Nat. Lond. 170 (1952) 1123.
[2] H.M. Widatallah, C. Johnson, F. Berry, M. Pekala, Solid State Commun. 120 (2001) 171–175.
[3] G.M. Argentina, P.D. Baba, IEEE Trans. Microw. Theory Tech. 22 (1974) 652–658.
[4] J.S. Baijal, S. Phanjoubam, D. Kothari, Solid State Commun. 83 (1992) 679–682.
[5] U. Lüders, A. Barthélémy, M. Bibes, K. Bouzehouane, S. Fusil, E. Jacquet, J.-P. Contour, J.-F. Bobo, J. Fontcuberta, A. Fert, Adv. Mater. 18 (2006) 1733–1736.
[6] M.G. Chapline, S.X. Wang, Phys. Rev. B 74 (2006) 014418.
[7] A.V. Ramos, M.-J. Guittet, J.-B. Moussy, R. Mattana, C. Deranlot, F. Petroff, C. Gatel, Appl. Phys. Lett. 91 (2007) 122107.
[8] G.O. White, C.E. Patton, J. Magn. Magn. Mater. 9 (1978) 299–317.
[9] S. Lefebvre, R. Portier, M. Fayard, Phys. Stat. Sol. A 24 (1974) 79–89.
[10] M. Brunel, F. De Bergevin, Solid State Commun. 4 (1966) 165–168.
[11] P.W. Anderson, Phys. Rev. 102 (1956) 1008–1014.
[12] J.L. Dormann, A. Tomas, M. Nogues, Phys. Stat. Sol. A 77 (1983) 611–618.
[13] C. Boyraz, D. Mazumdar, M. Iliev, V. Marinova, J. Ma, G. Srinivasan, A. Gupta, Appl. Phys. Lett. 98 (2011) 012507.
[14] N. Pachauri, B. Khodadadi, M. Althammer, A.V. Singh, B. Loukya, R. Datta, M. Iliev, L. Bezmaternykh, I. Gudim, T. Mewes, A. Gupta, J. Appl. Phys. 117 (2015) 233907.
[15] R.F. Egerton, Electron Energy-loss Spectroscopy in the Electron Microscope, Springer, New York, 2011.
[16] P. Blaha, K. Schwarz, G.K.H. Madsen, D. Kvasnicka, J. Luitz, WIEN2k: an Augmented Plane Wave + Local Orbitals Program for Calculating Crystal Properties, Karlheinz Schwarz, Techn. Universität Wien, Austria, 2001.
[17] F. Tran, P. Blaha, Phys. Rev. Lett. 102 (2009) 226401.
[18] R. Datta, S. Kanuri, S.V. Karthik, D. Mazumdar, J.X. Ma, A. Gupta, Appl. Phys. Lett. 97 (2010) 071907.
[19] R. Datta, B. Loukya, N. Li, A. Gupta, J. Cryst. Growth 345 (2012) 44–50.
[20] X.Z. Yu, T. Arima, Y. Kaneko, J.P. He, R. Mathieu, T. Asaka, T. Hara, K. Kimoto, Y. Matsui, Y. Tokura, J. Phys. Condens. Matter 19 (2007) 172203.
[21] R.G. Crespo, A.Y. Al-Baitai, I. Saadoune, N.H. De Leeuw, J. Phys. Condens. Matter 22 (2010) 255401.
[22] G.W. van Oosterhout, C.J.M. Rooijmans, Nature 181 (1958) 44.
[23] C.J. Greaves, J. Solid State Chem. 49 (1983) 325–333.
[24] A.N. Shmakov, G.N. Kryukova, S.V. Tsybulya, A.L. Chuvilin, L.P. Solovyeva, J. Appl. Crystallogr. 28 (1995) 141–145.
[25] X.L. Huang, Y. Yang, J. Ding, Acta Mater. 61 (2013) 548–557.
[26] J.E. Jorgensen, L. Mosegaard, L.E. Thomsen, T.R. Jensen, J.C. Hanson, J. Solid State Chem. 180 (2007) 180–185.
[27] H. Tian, J. Verbeeck, S. Brück, M. Paul, D. Kufer, M. Sing, R. Claessen, G. Van Tendeloo, Adv. Mater. 26 (2014) 461–465.